Controlling Product Selectivity During Dioxygen Reduction with Mn Complexes Using Pendent Proton Donor Relays and Added Base

Emma N. Cook, Ian M. Courter, Diane A. Dickie, and Charles W. Machan*

Department of Chemistry
University of Virginia
PO Box 400319 McCormick Rd, Department of Chemistry, University of Virginia, Charlottesville, VA, USA 22904-4319
E-mail: machan@virginia.edu

Abstract: The catalytic reduction of dioxygen (O_2) is important in biological energy conversion and alternative energy applications. In comparison to Fe- and Co-based systems, examples of catalytic O_2 reduction by homogeneous Mn-based systems is relatively sparse. Motivated by this lack of knowledge, two Mn-based catalysts for the oxygen reduction reaction (ORR) containing a bipyridine-based non-porphyrinic ligand framework have been developed to evaluate how pendent proton donor relays alter activity and selectivity for the ORR, where Mn($^{p\text{-}tbu}$dhbpy)Cl (**1**) was used as a control complex and Mn(^{nPr}dhbpy)Cl (**2**) contains a pendent –OMe group in the secondary coordination sphere. Using an ammonium-based proton source, *N,N′*-diisopropylethylammonium hexafluorophosphate, we analyzed catalytic activity for the ORR: **1** was found to be 64% selective for H_2O_2 and **2** is quantitative for H_2O_2, with O_2 binding to the reduced Mn(II) center being the rate-determining step. Upon addition of the conjugate base, *N,N′*-diisopropylethylamine, the observed catalytic selectivity of both **1** and **2** shifted to H_2O as the primary product. Interestingly, while the shift in selectivity suggests a change in mechanism for both **1** and **2**, the catalytic activity of **2** is substantially enhanced in the presence of base and the rate-determining step becomes the bimetallic cleavage of the O–O bond in a Mn-hydroperoxo species. These data suggest that the introduction of pendent relay moieties can improve selectivity for H_2O_2 at the expense of diminished reaction rates from strong hydrogen bonding interactions. Further, although catalytic rate enhancements are observed with a change in product selectivity when base is added to buffer proton activity, the pendent relays stabilize dimer intermediates, limiting the maximum rate.

Introduction

Increasing atmospheric CO_2 concentrations has led to global warming and climate change, creating an undeniable need for renewable energy processes. Activation and reduction of dioxygen (O_2) is an attractive route for the development of alternative energy and industrial-scale oxidation reactions due to its abundance and oxidizing power.[1-9] The oxygen reduction reaction (ORR) to the $4H^+/4e^-$ product, H_2O, is an ideal cathodic half reaction in hydrogen fuel cells and selectivity for the $2H^+/2e^-$ product, H_2O_2, is also attractive because of the large-scale use of H_2O_2 as an oxidant in a number of industrial processes.[2, 3, 7, 9-11] Molecular complexes offer a compelling way to study and optimize these electrocatalytic reactions because of the fidelity with which the active sites can be characterized relative to heterogeneous systems that may contain a distribution of active sites, as well as the possibility of using iterative synthetic modifications to test mechanistic hypotheses.

Interest in bioinspired and biomimetic systems has spurred the development of a significant number of Fe- and Co-based porphyrinic systems.[3, 9, 12, 13] By comparison, Mn has been less widely studied, despite its reactivity toward O_2 and prevalence in dioxygen-dependent biological systems.[1, 2, 9] Because of the relatively high spin-pairing energy of Mn ions, open-shell configurations with side-on coordination modes of O_2 are often observed to be relatively stable on the potential energy surface of catalytic reactions, limiting activity.[2, 14-16] This issue arises, in part, as a result of the low basicity of O atoms in side-on Mn–O_2 species, preventing effective protonation and cleavage of the O–O bond.[2, 14] This remains a challenge in the development of Mn-based catalysts for ORR, where destabilization of side-on Mn–O_2 intermediates (and other stable reactive oxygen species, ROSs) is crucial to achieve enhanced rates of catalytic turnover (**Figure 1**).[2, 14]

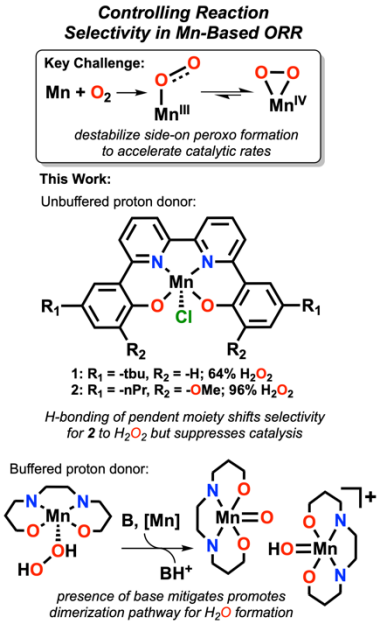

Figure 1. Summary of the work described here.

There are a number of strategies that can be employed to avoid stable Mn ROS intermediates, including synthetically modifying the supporting ligand framework to tune the electronic structure at the metal center, the introduction of hydrogen-bonding interactions that alter the potential energy surface for Mn–O_2 intermediates, or the use of steric hindrance at the active site.[2] For instance, to explore how secondary-sphere ligand modification influenced ORR activity and selectivity, Nocera and coworkers introduced a xanthene-based pendent hangman moiety in a Mn tetraphenylporphyrin complex for ORR.[17] They found that the hangman group promoted intramolecular proton transfer during catalysis and that hydrogen-bonding interactions between Mn-bound O_2 and proton donors helped to favor end-on coordination modes.[17] A firm fundamental understanding of how synthetic control over ORR at Mn-based active sites can avoid these potential thermodynamic limitations during catalysis remains an important question. Among the reports on Mn-based ORR catalysts, there are only a handful of non-porphyrinic based systems, despite the possibilities for alternative synthetic approaches for reaction control.[2, 18-23]

Previous studies on the electrochemical ORR mediated by Co(N_2O_2) molecular complexes with 2,2′-bipyridine based ligand backbone[24] found that the introduction of a –OMe pendent relay in the secondary coordination sphere resulted in a shift in selectivity from H_2O to H_2O_2, as well as a shift in the observed RDS based on acid strength.[25] It was hypothesized that directed protonation of the proximal oxygen of a Co–OOH intermediate was mediated by the pendent –OMe group.[25] Reasoning that pendent relays could favor end-on O_2 coordination and accelerate proton transfer in analogous Mn-based systems,[22, 23, 26] two new Mn-based non-porphyrinic electrocatalysts for ORR have been prepared. Using an alkyl ammonium-based proton source, it was found that a secondary sphere –OMe pendent relay shifts selectivity to quantitative H_2O_2 formation under unbuffered conditions (proton donor is present without its conjugate base), although the rate of catalysis is suppressed. However, under buffered conditions (the proton donor and its conjugate base are present in significant quantities), hydrogen bonding between the ligand framework and the added acid is mitigated, resulting in a dramatic increase in rate and a shift in selectivity to H_2O production. Interestingly, the shift in selectivity occurs in complexes with and without the pendent relay, with systematic variation of added base concentration implying that the change in mechanism is related to the deprotonation of a Mn hydrogen peroxide intermediate. Further, the complex with the pendent relay experiences a shift in rate-determining step (RDS) for catalysis under buffered conditions, which is proposed to originate from the pendent relay stabilizing Mn dimer formation relative to O_2 binding and activation.

Overall, the proposed mechanism suggests that the $4H^+/4e^-$ product H_2O is accessed by deprotonating an intermediate hydrogen peroxide species, implying that proton activity buffering at the pK_a of relevant intermediates is a potential point of reaction control over the selectivity of product formation, as well as a

mode of control over hydrogen-bonding interactions. These observations are representative of the complexity of ORR with Mn active sites: proton transfer is required to facilitate the reduction of superoxide to hydroperoxide (which we attribute to the competition between end-on and side-on coordination modes), but O–O bond scission occurs most efficiently from a hydroperoxo intermediate.

Results and Discussion

Synthesis and Characterization

The $^{p\text{-}tbu}$dhbpy[H]$_2$ and ^{nPr}dhbpy[H]$_2$ ligands were synthesized according to previously reported procedures.[25] Metalation of $^{p\text{-}tbu}$dhbpy[H]$_2$ to generate Mn($^{p\text{-}tbu}$dhbpy)Cl **1** was achieved via a modified literature procedure,[22] where a stoichiometric amount of manganese(II) acetate tetrahydrate was sparged with compressed air, allowed to reflux with $^{p\text{-}tbu}$dhbpy[H]$_2$ for 3 hours in MeOH solution, and induced to precipitate by the addition of a saturated NaCl solution. Metalation of ^{nPr}dhbpy[H]$_2$ was achieved by an analogous synthetic procedure.

UV-vis, ESI-MS, and microanalyses are consistent with the proposed formulation of the Mn complexes shown in **Figure 1**. Evans' method measurements exhibited $\mu_{eff} = 4.78 \pm 0.11$ and $\mu_{eff} = 4.59 \pm 0.10$ for **1** and **2**, respectively; both values are consistent with high-spin d^4 Mn(III) complexes (**Tables S1** and **S2**).[27, 28] Single crystals suitable for X-ray diffraction studies of complex **2** were grown by slow cooling of a saturated, boiling acetonitrile (MeCN) solution layered with diethyl ether. The solid-state structure of **2** is a dimeric species where a single O atom from each atom is coordinated in the axial position of a second equivalent of complex **2** to create a six-coordinate environment for each Mn center, analogous to our previous studies on a comparable Fe complex (**Figures 2C-2D**).[29]

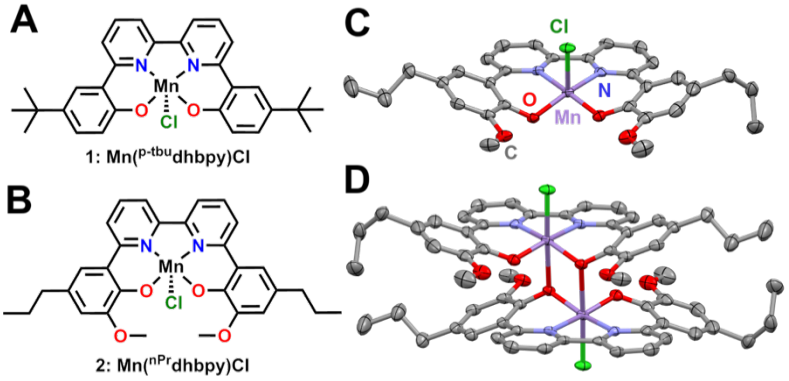

Figure 2. (A) Structure of **1** Mn($^{p\text{-}tbu}$dhbpy)Cl, (B) structure of **2** Mn(^{nPr}dhbpy)Cl, (C) Molecular structure of Mn(^{nPr}dhbpy)Cl **2** from single crystal X-ray diffraction studies showing the (D) dimeric solid-state species. Purple = Mn, red = O, green = Cl, gray = C; thermal ellipsoids 50%, H atoms and disordered atoms omitted for clarity. CCDC 2255849.

Diisopropylethylammonium hexafluorophosphate ($DIPEAHPF_6$) was synthesized according to a previously reported procedure.[30] Toluene was brought to reflux in the presence of ammonium hexafluorophosphate (PF_6) and diisopropylethylamine (DIPEA), resulting in the precipitation of a solid product after 48 hours. The suspension was cooled to 0° C on an ice bath before being filtered and washed with DCM. Rotary evaporation of the DCM solvent yielded a spectroscopically pure product: NMR spectroscopic characterization and microanalysis were consistent with a disopropylethylammonium salt with a PF_6^- counteranion. Single crystals suitable for X-ray diffraction studies were grown via slow evaporation from a concentrated DCM solution (**Figure S3**). ^{1}H NMR spectroscopy was used to estimate a pK_a of 18.7 for $DIPEAHPF_6$ in MeCN via titration and competition experiments (See SI).[31]

Electrochemical Analysis of 1 and 2

Cyclic voltammetry studies were performed on **1** and **2** in MeCN solution with 0.1 M tetrabutylammonium hexafluorophosphate ($TBAPF_6$) supporting electrolyte (**Figure 3**). Under an inert Ar atmosphere, **1** (**Figure S9**) and **2** (**Figure S16**) show reversible features attributed to a Mn(III/II) redox event at –0.58 and –0.55 V vs. Fc^+/Fc, respectively. Variable scan-rate studies of both **1** and **2** under Ar gas saturation showed a diffusion-limited response, consistent with homogenous species (**Figures S8** and **S15**, respectively). Upon dioxygen (O_2) saturation, there is an observed slight increase in current density at the Mn(III/II) redox event as well as the partial loss of the return oxidation feature for both **1** (**Figure S9**) and **2** (**Figure S16**), indicative of a reaction involving O_2 and the reduced Mn(II) metal center. Conversely, there is a quasi-reversible redox feature observed at more negative potentials for **2** under O_2 saturation, suggestive of a Mn superoxide/peroxide reduction following O_2 binding and activation.

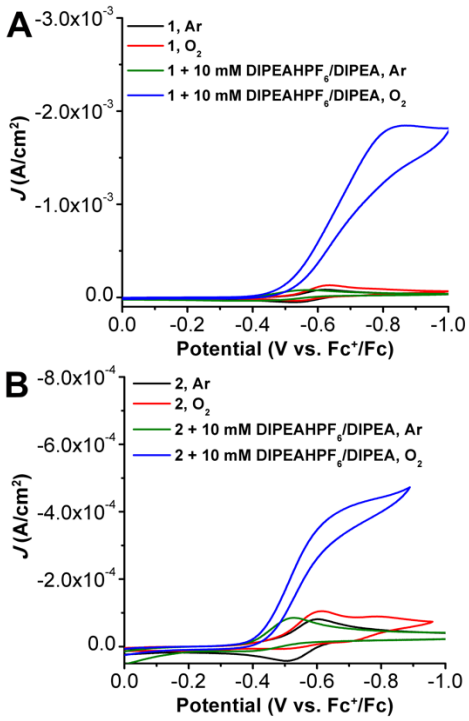

Figure 3. (A) CVs of Mn($^{p\text{-}tbu}$dhbpy)Cl **1** under Ar and O_2 with and without 10 mM DIPEAHPF$_6$/DIPEA present. (B) CVs of Mn(^{nPr}dhbpy)Cl **2** under Ar and O_2 with and without 10 mM DIPEAHPF$_6$/DIPEA present. Conditions: 0.5 mM Mn, 0.1 M TBAPF$_6$/MeCN; glassy carbon working electrode, glassy carbon rod counter electrode, Ag/AgCl pseudoreference electrode; referenced to Fc^+/Fc internal standard; 100 mV/s scan rate.

Initial addition of 10 mM of the DIPEAHPF$_6$ proton donor to both **1** and **2** under inert conditions resulted in the loss of reversibility of the Mn(III/II) redox couple as well as a shift to more positive potentials, $E_{p,a}$ = –0.56 V vs Fc^+/Fc for **1** (**Figure S9**) and –0.53 V vs Fc^+/Fc for **2** (**Figure S16**). This is consistent with a contribution from an *EC* mechanism (reversible electron transfer followed by an irreversible chemical reaction), which is proposed to be the protonation of an O atom in the inner-coordination sphere following formal reduction to Mn(II), consistent with our previous studies on acids with similar pK_a values.[22, 32] Although titration of increasing amounts of DIPEAHPF$_6$ beyond 10 mM did not cause a further potential shift for **1**, the maximum positive potential shift for **2** was reached after the addition of 20 mM. Similarly, titration of increasing amounts of the DIPEAHPF$_6$ proton donor in the presence of 10 mM DIPEA revealed that the Mn(III) reduction potential observed for **1** and **2** shifted to more positive potentials, however this shift was not dependent on the concentration of DIPEAHPF$_6$ (**Figures S11** and **S17**).

The observation of these shifts in the presence of the proton donor and its conjugate base, as well as the absence of a Nernstian relationship suggested that the axial chloride ligand was participating in related chemical steps during the *EC* mechanism. To better understand the role of DIPEA and DIPEAHPF$_6$ in axial

Cl^- ligand solvation, CVs of **1** (**Figure S13** and **S14**, respectively) were taken in the presence of 0.1 M TBACl. The addition of increasing amounts of both DIPEA by itself and $DIPEAHPF_6$ with a fixed concentration of DIPEA (buffered) in the presence of excess Cl^- under Ar saturation conditions suppressed positive potential shifts of the Mn(III/II) redox feature in **1**. The suppression of the potential shift in the presence of excess Cl^- suggests that the shift observed originally is due to axial ligand solvation. Since it was observed that increasing concentrations of $DIPEAHPF_6$ led to a loss of reversibility for the Mn(III/II) feature, these data taken in aggregate imply that axial Cl^- ligand loss enables protonation of the O atom in the inner coordination sphere upon reduction.

Similar studies were conducted on **2**, where the addition of 0.1 M TBACl to a solution of **2** resulted in a negative potential shift of a quasireversible Mn(III/II) feature to –0.76 V vs. Fc^+/Fc (**Figure S22)**. Addition of 10 mM DIPEA caused a positive potential shift of this Mn(III/II) redox feature back to –0.56 V vs. Fc^+/Fc (**Figure S22**) and the titration of increasing amounts of $DIPEAHPF_6$ under buffered conditions suppressed the observed positive potential shift (**Figure S23**). As was the case with complex **1**, it is hypothesized that the presence of both DIPEA and $DIPEAHPF_6$ contribute to axial Cl^- ligand loss for **2**, with irreversibility again suggesting protonation of a ligand O atom bound to Mn. Consistent with this, UV-vis spectroscopic analysis of **1** and **2** in the presence of DIPEA and $DIPEAHPF_6$ showed no evidence of interaction with Mn(III) (**Figures S58-S61**).

Under O_2 saturation in the presence of 10 mM $DIPEAHPF_6$, there is an increase in current at the Mn(III/II) reduction feature for both **1** (**Figure S9**) and **2** (**Figure S16**), indicative of electrocatalytic activity for the ORR. Likewise, under O_2 saturation in the presence of buffered $DIPEAHPF_6$ (1:1 ratio of ammonium to its conjugate base), there is an increase in current density at the Mn(III/II) redox couple for both **1** and **2**, consistent with catalytic O_2 reduction (**Figure 3**). Effective overpotentials (η) for the ORR by **1** and **2** calculated under buffered conditions were determined to be 0.58 and 0.56 V, respectively. Notably, the catalytic current density observed under buffered conditions with complex **2** is much higher than unbuffered conditions (**Figure S19**), suggesting that the presence of conjugate base enhances electrocatalytic ORR by **2**, *vide infra*. Oxidative current due to amine oxidation precludes the use of rotating ring-disk methods for H_2O_2 detection under these conditions for both **1** and **2** (**Figure S24**).

Spectrochemical Studies with 1 and 2

Catalytic ORR experiments with **1** and **2** were then run under spectrochemical conditions using decamethylferrocene (Cp^*_2Fe) as a chemical reductant in solution with the DIPEAH proton donor under unbuffered and buffered (1:1 ratio of $DIPEAHPF_6$ to DIPEA) conditions. UV-vis stopped-flow spectroscopy was used to determine the kinetic parameters of the ORR by monitoring the accumulation of oxidized $[Cp^*_2Fe]^+$ at 780 nm (Figure 4). Consistent with the electrochemical data, ORR by 1 showed minimal differences in activity under catalytic conditions with buffered and unbuffered proton donor

(Figure 4A). Likewise, the catalytic response mediated by 2 showed a significant enhancement under buffered conditions compared to unbuffered (Figure 4B), similar to what was observed under electrochemical conditions, *vide supra*.

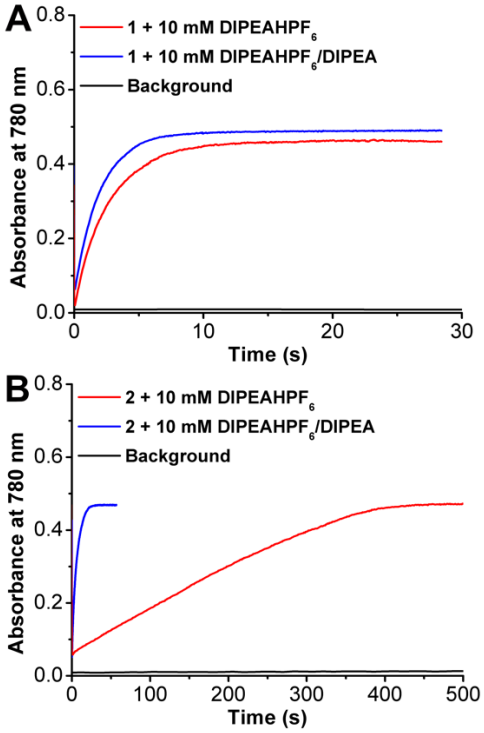

Figure 4. Change in absorbance at 780 nm over time as a result of the formation of $[Cp^*_2Fe]^+$ by ORR catalyzed by Mn($^{p\text{-}tbu}$dhbpy)Cl **1** (**A**) with $DIPEAHPF_6$ (red) and $DIPEAHPF_6$/DIPEA (blue) and Mn(^{nPr}dhbpy)Cl **2** (**B**) with $DIPEAHPF_6$ (red) and $DIPEAHPF_6$/DIPEA (blue). Black: buffered control. Conditions: 40 µM [Mn], 4.05 mM [O_2], 1 mM [Cp^*_2Fe], 10 mM [$DIPEAHPF_6$/DIPEA]; control: 4.05 mM O_2, 1 mM Cp^*_2Fe, 12.5 mM $DIPEAHPF_6$/DIPEA.

Variable concentration studies with **1** and $DIPEAHPF_6$ under unbuffered conditions revealed a rate law for the ORR with first-order dependencies on [**1**] and [O_2] and zero-order dependencies on [$DIPEAHPF_6$] and [Cp^*_2Fe] (**Figures S36-S39**), corresponding to the rate law shown in **Eq (1)**.

$$rate_{unbuffered} = k_{cat}[Mn^{p-tbu}]^1[O_2]^1 \quad \textbf{Eq (1)}$$

A $Ti(O)SO_4$ colorimetric assay was used to determine the selectivity of the ORR as previously described.[23, 33] Aliquots were taken after the reaction was allowed to reach completion and the amount of H_2O_2 produced was quantified. Selectivity testing under unbuffered conditions revealed that **1** is 64.2 ± 6.9% selective for H_2O_2 corresponding to an n_{cat} of 2.72 (**Figure S26** and **Table 1**). Under these unbuffered

conditions (only proton donor present), control studies showed no degradation of H_2O_2 via disproportionation, with quantitative recovery of H_2O_2 (**Figure S28** and **Table S6**).

Similarly, variable concentration studies of ORR by **2** with unbuffered DIPEAHPF$_6$ showed first-order dependencies on [**2**] and [O_2] (**Figures S45-S49**). Selectivity studies showed 96.2 ± 4.1% H_2O_2 selectivity corresponding to an n_{cat} = 2.08 (**Figure S27** and **Table S5**), with control studies showing that 93.6 ± 4.6% H_2O_2 was recovered after 20 minutes (**Figure S29** and **Table S7**), consistent with very slight activity for H_2O_2 disproportionation. Notably, the observation of an increased amount of the H_2O_2 product for complex **2** – which contains pendent proton donor relays – mirrors similar observations made with Co-based analogues of these compounds previously.[25] Thus, **Eq (2)** is proposed as the rate law for ORR mediated by **2** under unbuffered conditions.

$$rate_{unbuffered} = k_{cat}[Mn^{nPr}]^1[O_2]^1 \qquad \textbf{Eq (2)}$$

Subsequent re-examination of **1** under buffered conditions (equal amounts of ammonium proton donor and its conjugate base) showed first-order dependencies on [**1**] and [O_2] and zero-order dependencies on [1:1 DIPEAHPF$_6$:DIPEA] and [Cp*$_2$Fe] (**Figures S40-S44**). Systematically varying the concentration of either [DIPEAHPF$_6$] or [DIPEA] against a fixed concentration of the other also exhibited no concentration dependence on the catalytic reaction (**Figure S42**). Selectivity studies revealed that after 15 s, **1** showed 81.9 ± 4.1% selectivity for H_2O as the product (**Figure S30** and **Table 1**). H_2O_2 disproportionation was observed under catalytic conditions: only 10.8 ± 6.6% H_2O_2 was recovered after 105 s with 1:1 DIPEAHPF$_6$:DIPEA present (**Figure S32** and **Table S10**). Interestingly, control studies under buffered catalytic conditions without the presence of O_2 revealed minimal degradation of H_2O_2 by the Mn(II) form of the complex (**Figure S34** and **Table S12**), suggesting that the observed reaction selectivity difference is not due to disproportionation alone. These results are summarized in the following rate law, **Eq (3)**, for ORR mediated by **1** under buffered conditions:

$$rate_{buffered} = k_{cat}[Mn^{p-tbu}]^1[O_2]^1 \qquad \textbf{Eq (3)}$$

Conversely, variable concentration studies of ORR catalyzed by **2** under buffered conditions revealed mechanistic differences in comparison to the data obtained for **1** and **2** under unbuffered conditions, as well as a change in selectivity. The ORR mediated by **2** showed a second-order dependence on [**2**], a first-order dependence on [1:1 DIPEAHPF$_6$:DIPEA], an inverse first-order dependence on [Cp*$_2$Fe] and a zero-order dependence on [O_2] (**Figures S49-S53**). Unlike **1**, when [DIPEA] was varied against a fixed concentration of [DIPEAHPF$_6$] with **2**, a first-order dependence on rate was observed; experiments where [DIPEAHPF$_6$]

was varied against a fixed [DIPEA] showed a zero-order dependence. These results lead to the proposed rate law shown in **Eq (4)**. The observed first-order dependence on [DIPEA] implies that the dependence observed on [1:1 $DIPEAHPF_6$:DIPEA] is a result of varying DIPEA concentration. This interpretation is validated by the zero-order dependence on [$DIPEAHPF_6$] with fixed [DIPEA], ruling out proton activity or proton donor concentration as influencing the observed reaction rate.

$$rate = k_{cat}[Mn^{nPr}]^2[DIPEA]^1[Cp^*_2Fe]^{-1} \qquad \textbf{Eq (4)}$$

Selectivity studies of ORR under buffered conditions showed that after 15 s, **2** is 62.1 ± 6.7% selective for H_2O (**Figure S33** and **Table 1**). Control studies showed H_2O_2 degradation consistent with disproportionation: after 150 s only 3.81 ± 0.83% of H_2O_2 was recovered under buffered conditions with complex **2**. Again, H_2O_2 reduction was not observed under the buffered catalytic conditions when placed under an inert N_2 atmosphere, suggesting that the change in selectivity is not exclusively due to disproportionation (**Figure S35** and **Table S13**).

Table 1. Summary of ORR selectivity under spectrochemical conditions of 1 and 2 under unbuffered and buffered conditions.

	Unbuffered		Buffered (15 s)	
	% H_2O_2	%H_2O	%H_2O_2	%H_2O
1	64.2 ± 6.9	35.8 ± 6.9	18.1 ± 4.1	81.9 ± 4.1
2	96.2 ± 4.1	3.8 ± 4.1	37.9 ± 6.7	62.1 ± 6.7

Computational Studies on Complex 2

To evaluate the initial steps of the reaction, computational studies on the thermodynamic positioning of likely intermediates for complex **2** during O_2 reduction to H_2O_2 were subsequently undertaken (see SI for details). Geometry optimization was done with the Gaussian 16 package[34] at B3LYP-D3(BJ)/def2-SVP level[35-42] with a complete structural model and single point calculations for refining energy differences were completed with Orca 5.0[43] at the ωB97M-D4/def2-TZVPP level.[39, 40, 44-48] At this level of theory, the calculated reduction potential of –0.53 V vs $Fc^{+/0}$ showed satisfactory agreement with the experimental potential of –0.55 V. Further, the anticipated ground states of S=2 for Mn(III) and S=5/2 for Mn(II) in this coordination environment were accurately reproduced, lending confidence to the chosen method.[22] Electron transfer-proton transfer (ET-PT), proton transfer-electron transfer (PT-ET), and concerted electron-proton transfer (CEPT) pathways for reaction steps where a net hydrogen atom transfer occurred were considered; in all cases CEPT was found to be the most favorable and produced results consistent with experimental observation.

The most probable thermodynamic step from the starting complex $[Mn(^{nPr}dhbpy)(Cl)]^0$ under protic conditions is reduction followed by a hydrogen-bonding interaction between the ligand framework and an equivalent of $[DIPEAH]^+$ to generate $[Mn(^{nPr}dhbpy[AH])(Cl)]^0$. (**Figure 5**). Note that the [AH] notation indicates the hydrogen-bonding interaction involving a Mn-bound O atom from the ligand framework. Although formal proton transfer to the ligand framework with loss of DIPEA is exergonic by –7.2 kcal/mol, the binding of O_2 with accompanying Cl^- release to generate the cationic species $[Mn(^{nPr}dhbpy[H])(\eta^2\text{-}O_2)]^+$ is uphill by 34.2 kcal/mol, precluding its involvement in the catalytic cycle. Instead, O_2 binding with loss of [DIPEAH][Cl] is endergonic by 20.2 kcal/mol, which is consistent with experimental observations, generating $[Mn(^{nPr}dhbpy)(\eta^2\text{-}O_2)]^0$. In this structure, the bound O_2 is in a side-on coordination mode with a bond length of 1.309 Å, consistent with reduction to superoxide, $O_2^{\bullet-}$. Reduction and protonation of this species had a favorable CEPT pathway (–0.01 V vs $Fc^{+/0}$), where proton transfer has occurred from $[DIPEAH]^+$ to generate $[Mn(^{nPr}dhbpy)(\eta^1\text{-}O_2H)]^0$. The shift in coordination mode of the O_2 fragment from side-on to end-on reflects additional reduction: the bond lengthens to 1.451 Å, consistent with a peroxide. Protonation of the proximal O atom to generate $[Mn(^{nPr}dhbpy)(\eta^1\text{-}O_2H_2)]^+$ by an equivalent of $[DIPEAH]^+$ is endergonic by 9.9 kcal/mol and displacement by Cl^- to facilitate H_2O_2 release is favorable by –23.6 kcal/mol. These reaction steps align with experimental observations on the catalytic cycle which produces H_2O_2 under unbuffered conditions.

Next the favorability of dimerization from the hydroperoxide was assessed to explore the implied dimeric pathway to H_2O production (**Figure S77**). The experimental studies described above established the viability of H_2O_2 as an intermediate species, therefore the $[Mn(^{nPr}dhbpy)(\eta^1\text{-}O_2H_2)]^+$ adduct was considered as the starting point. Deprotonation of Mn-bound H_2O_2 by DIPEA to generate $[Mn(^{nPr}dhbpy)(\eta^1\text{-}O_2H)]^0$ is favorable by 9.9 kcal/mol. Subsequent dimerization of $[Mn(^{nPr}dhbpy)(\eta^2\text{-}O_2H)]^0$ with an equivalent of $[Mn(^{nPr}dhbpy)(Cl)]^0$ is endergonic by 19.7 kcal/mol, generating $[Mn(^{nPr}dhbpy)(O)]^0$ (S=3/2), $[Mn(^{nPr}dhbpy)(OH)]^+$ (S=3/2), and Cl^- as the products. Attempts to examine a stabilized bridging hydroperoxo dimer were unsuccessful, homolytic O–O bond scission occurred spontaneously in all cases. From the terminal manganese oxo $[Mn(^{nPr}dhbpy)(O)]^0$, a calculated CEPT potential of +1.00 V vs Fc^+/Fc was obtained for the production of a Mn(III) hydroxide $[Mn(^{nPr}dhbpy)(OH)]^0$, while the convergent pathway via the reduction of $[Mn(^{nPr}dhbpy)(OH)]^+$ was estimated to be +0.62 V; both processes are expected to be facile at the considered operating potential of –0.55 V vs Fc^+/Fc. Protonation of the neutral Mn–OH species to make the corresponding aquo species is uphill by 1.2 kcal/mol and subsequent H_2O loss with Cl^- coordination to Mn to regenerate the starting species and close the H_2O_2 reduction cycle is downhill by –20.2 kcal/mol.

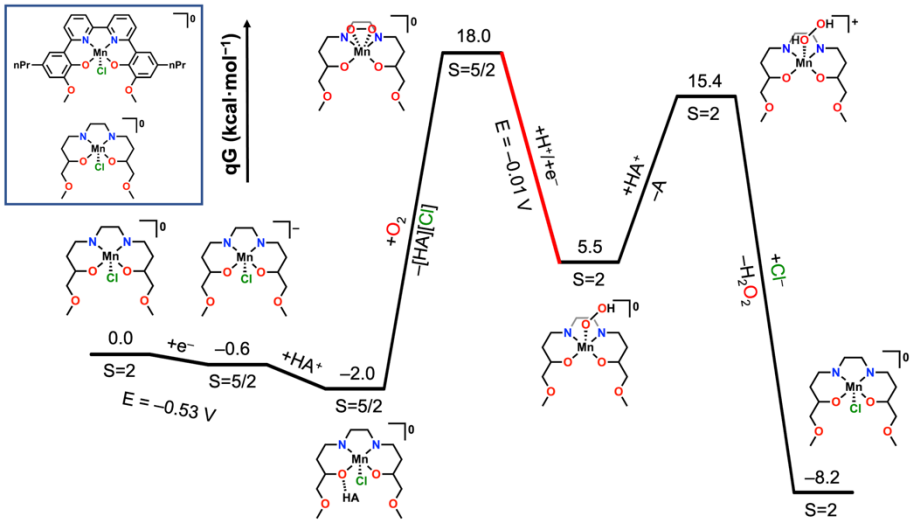

Figure 5. Free energy diagram from DFT methods showing key thermodynamic intermediates in the production of H_2O_2 by complex **2**. Diagram considers the operating potential of catalysis to be –0.55 V vs $Fc^{+/0}$ and red indicates CEPT steps. DIPEA = A and $DIPEAH^+ = HA^+$.

Discussion

From the data summarized above, we are able to propose the following mechanisms for the ORR catalyzed by **1** and **2** under unbuffered and buffered conditions, described in **Scheme 1**. Starting at *i*, the reduction of Mn(III) to Mn(II) induces a hydrogen-bonding interaction between $[DIPEAH]^+$ and the O atom in the inner coordination sphere to form *ii*, the resting state of the catalyst in solution. It is likely that this species exists in equilibrium with formal proton transfer, based on DFT results, UV-vis studies on chemically reduced species (**Figures S64** and **S71**), and the observed irreversibility of the Mn(III)/(II) reduction. Control studies showed that neither $DIPEAHPF_6$ or DIPEA interacted substantially with complexes in the Mn(III) oxidation state (**Figures S58-S61**). However, formal proton transfer renders O_2 binding to Mn less favorable by 14 kcal/mol according to DFT methods, indicating that this pathway isn't viable catalytically.

Scheme 1. Proposed catalytic cycle for ORR, with the key equilibrium for switching between the two reaction pathways indicated in gray.

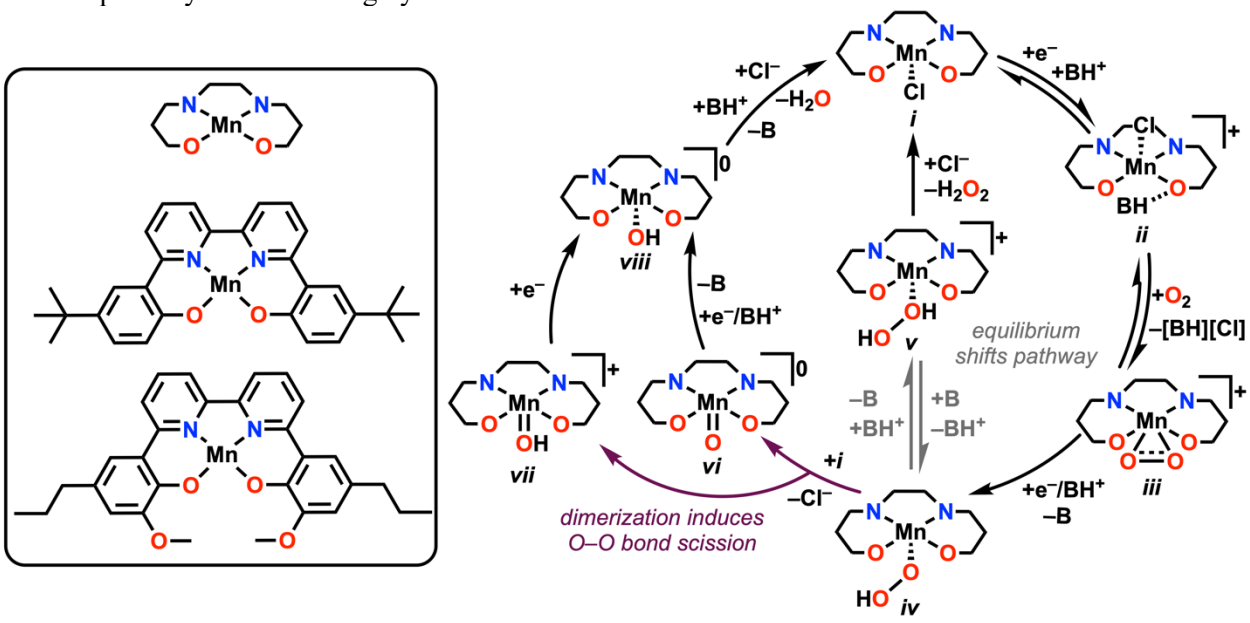

Following this activation of the catalyst, rate-limiting O_2 binding to Mn(II) to form a Mn(III)-superoxide species, *iii*, occurs with loss of [DIPEAH][Cl]. Based on this assignment, species *ii* is considered to be the resting state of the catalytic cycle under these conditions. Reduction and protonation by a CEPT pathway results in the formation of a Mn-hydroperoxo species, *iv*, whose protonation leads to the formation of a Mn–H_2O_2 intermediate, *v*. This is the primary reaction pathway for **1** (64.2 ± 6.9% selectivity) and **2** (96.2 ± 4.1% selectivity) under unbuffered conditions, as suggested by selectivity studies and the relative absence of activity for H_2O_2 disproportionation in separate testing. The observed selectivity enhancement for H_2O_2 during ORR mediated by **2** is consistent with the participation of the pendent methoxy group in hydrogen bonding interactions with added acid, as we have observed previously.[25] This mechanistic proposal is consistent with the general thermodynamic landscape obtained by DFT methods (**Figure 5**). It is worth noting that H_2O_2 disproportionation is observed by the parent Mn(III) species of both complexes in the presence of DIPEA. Further, control studies with Mn(II) revealed minimal interaction with H_2O_2 (**Figure S34**), suggesting that disproportionation is reliant on the availability of formally Mn(III) complexes.

Under buffered conditions, complex **2** demonstrated a substantial increase in the observed catalytic rate in comparison to unbuffered conditions with an accompanying mechanistic divergence involving dimerization. While we do not observe a change in the rate-determining step or infer a change in the resting state for **1**, it is proposed that the shift in selectivity from H_2O_2 under unbuffered conditions to H_2O under buffered conditions is similarly due to the accessibility of a dimerization pathway in the presence of added

base. Based on the experimental and computational data presented, it is likely that the observed mechanistic divergence arises from differences in equilibrium control over the speciation of complexes *iv* and *v*, as depicted in **Eq (5)**.

$$Mn(O_2H) + BH^+ \rightleftharpoons [Mn(H_2O_2)]^+ + B \qquad \textbf{Eq (5)}$$

Therefore, under buffered conditions, an alternative reaction pathway dominates the observed selectivity. With suitable concentrations of base present, **Eq (5)** shifts to the left, favoring the hydroperoxo species, *iv*, which becomes the resting state for **2** under buffered conditions. Species *iv* dimerizes with an equiv of the Mn(III) complex *i* leading to the formation of species *vi* and *vii* from spontaneous O–O bond cleavage, with accompanying chloride loss. Following one-electron reduction or a one-electron CPET process, these products converge at a Mn(III) hydroxide species *viii*. Following this, formal protonation and displacement of H_2O by Cl^- complete the catalytic cycle. For complex **2**, O–O bond cleavage from dimerization becomes the RDS of the reaction, which is attributed to the pendent relay groups impacting dimerization through intermolecular coordination and hydrogen bonding. This proposal is consistent with the second-order rate dependence on [Mn] and first-order rate dependence on [DIPEA] under buffered conditions. Further, the inverse first-order dependence observed for [Cp*$_2$Fe] implies that Mn(III) is required for dimer formation, rather than Mn(II). This reaction pathway is in good agreement with that computed using DFT methods (**Figure S77**).

The differences in ORR catalyzed by **2** under unbuffered and buffered conditions in comparison to **1** suggest an important role for the pendent –OMe moiety in the secondary coordination sphere, as well as for the added base. Under unbuffered conditions, catalytic activity of **2** is suppressed in comparison to **1**, which is observed under both electrochemical and spectrochemical conditions. This is attributed to strong hydrogen-bonding interactions between the –OMe groups and $DIPEAHPF_6$ kinetically inhibiting O_2 binding, the rate-determining step of the catalytic cycle. In addition to catalytic suppression, we observe a shift in selectivity from approximately 64% for H_2O_2 by **1** to 96% for H_2O_2 by **2** under unbuffered catalytic conditions. As introduced above, we propose that the observed shift in product selectivity is due to the hydrogen-bonding interaction of the –OMe group assisting in proton transfer to the proximal Mn–OOH oxygen in species *iv*, as we have previously suggested in similar Co systems.[25]

Interestingly, upon the addition of the DIPEA conjugate base to catalytic conditions with **2**, catalysis is significantly enhanced under electro- and spectrochemical conditions. There is an accompanying change in mechanism, where the equilibrium responsible for H_2O_2 formation becomes unfavorable, allowing dimerization with accompanying O–O bond scission to become rate-determining. It is also likely that DIPEA mitigates the effects of the strong H-bonding interaction between $DIPEAHPF_6$ and the –OMe moiety, allowing an increased rate of hydroperoxo intermediate generation. Indeed, in control studies with **2** chemically reduced to Mn(II) by $CoCp_2$ *in situ,* the addition of $DIPEAHPF_6$ inhibited

reactivity with O_2: under unbuffered conditions the reaction between **2** and O_2 took approximately 100 min to go to completion (**Figure S72**), compared with approximately 25 m for complex **1** (**Figure S65**). It is also worth noting the difference in selectivity under buffered conditions between **1** and **2**, where **1** is 81.9% selective for H_2O (**Table 1**) and **2** is only 62.7% selective for H_2O. We attribute this difference to the H-bonding ability of the –OMe groups of **2** promoting the formation of species *v* during catalysis by directing the proton donor. However, the dimer pathway to water formation is the primary pathway under buffered conditions, as evidenced by the shift in observed rate law and the shift in product selectivity to H_2O.

The observed rate constants (R_{fit}/n_{cat} values) under identical buffered conditions for **1** and **2** were k_{obs} = 1.23 ± 0.17 x 10^{-1} s^{-1} and k_{obs} = 0.706 ± 0.25 x 10^{-1} s^{-1}, respectively. While addition of one equivalent of conjugate base for every equivalent of proton donor mitigates some of the hydrogen-bonding induced suppression observed for **2** under unbuffered conditions, the accompanying stabilization of the intermediate dimer results in a slight decrease in the rate of catalysis relative to **1**. Therefore, it has been demonstrated that the introduction of a pendent relay into homogeneous molecular Mn-based electrocatalysts plays an essential role in ORR through the hydrogen bond-assisted stabilization of key intermediates and by favoring the direct protonation of the proximal oxygen of the Mn-OOH intermediate. The relative hydrogen-bond donor ability of $DIPEAHPF_6$ is such that inhibition of catalysis can also occur, which is mitigated through the introduction of the conjugate base. However, the mitigation of this effect results in a change in mechanism, where O–O bond scission occurs spontaneously after dimerization. Thus, the conjugate base plays an important role during catalysis, allowing for an on-cycle dimer pathway that shifts the reaction pathway towards the formation of water.

It is worth briefly discussing the comparison between the data reported here for **1** and those reported previously with phenolic proton donors for a related complex with additional *tert*-butyl substituents.[22, 23] With buffered phenolic proton donors, the observed rate law for the ORR mediated by this more sterically hindered complex showed first-order dependencies on the on [catalyst] and [O_2], but no dependence on proton donor activity. Similarly, the results obtained in the presence of a buffered ammonium proton donor with higher activity (pK_a(MeCN) = 18.7) described here again demonstrate that proton activity is not relevant to the observed rate laws. The observed relevance of an off-cycle *EC* reaction involving the protonation of the ligand framework also aligns with the results of a potential-pK_a diagram obtained during the previous study where acids with pK_a < 20.11 were found to protonate the ligand framework of the tetra *tert*-butylated complex. The systems reported here show greater stability with respect to any H_2O_2 generated, which we had previously observed not to be the case in the presence of phenol and phenolate derivatives, consistent with the ease with which they can be oxidized as well as their competency as ligands relative to the sterically hindered ammonium/amine pairs used here.[50, 51] Indeed, control testing shows that

the DIPEA does not react under experimental conditions (**Figures S58-S59**) and is too sterically hindered to coordinate to Mn.

Conclusion

Here we report the synthesis and characterization of two new Mn(N_2O_2) homogeneous catalysts for ORR with an ammonium-based proton source in MeCN solution. Introduction of a pendent –OMe group in the secondary coordination sphere proved to play an important role during catalysis. Under unbuffered conditions, the pendent relay enabled quantitative selectivity for H_2O_2 due to directed protonation of the proximal O atom in a key Mn(III)–OOH intermediate. However, strong hydrogen-bonding interactions between the proton source and the pendent –OMe moiety suppressed catalytic activity. The addition of the proton donor's conjugate base enhanced the catalytic response and shifted the rate-determining step to O–O bond cleavage via Mn dimerization. These results describe the importance of secondary sphere ligand modifications in the tunability of catalytic ORR mediated by Mn complexes, including the role of hydrogen-bond donor ability in directing product selectivity and the benefits of buffered conditions. Destabilization of certain Mn–O_2 intermediates can be achieved through secondary sphere modifications, however, later steps in the catalytic cycle must also be considered, since they can impact in negative ways. The continued challenge for improved Mn-based ORR catalysts is to drive the initial O=O reduction with a proton donor while retaining activity for subsequent O–O bond scission. Based on these conclusions, we are exploring the use of proton relays with variable basicity in ligand frameworks which disfavor dimerization, in order to improve the activity of monomeric catalyst pathways mediated by Mn complexes.

Supporting Information

Computational coordinates, experimental and computational details, as well as supplementary data from additional cyclic voltammetry, spectrochemical, spectroscopic experiments are available. Deposition numbers 2255849 and 2255850 contain the supplementary crystallographic data for this paper. These data are provided free of charge by the joint Cambridge Crystallographic Data Centre.

Acknowledgements

We thank the University of Virginia for infrastructural support. E.N.C, I.M.C., and C.W.M. acknowledge N.S.F. CHE-2102156 for support. Single crystal X-ray diffraction experiments were performed on a diffractometer at the University of Virginia funded by the NSF-MRI program (CHE-2018870).

References

1. Cook, E. N.; Machan, C. W. Bioinspired mononuclear Mn complexes for O2 activation and biologically relevant reactions. *Dalton Transactions* **2021,** 50 (46), 16871-16886 DOI: 10.1039/D1DT03178C.
2. Cook, E. N.; Machan, C. W. Homogeneous catalysis of dioxygen reduction by molecular Mn complexes. *Chemical Communications* **2022,** 58 (84), 11746-11761 DOI: 10.1039/D2CC04628H.
3. Pegis, M. L.; Wise, C. F.; Martin, D. J.; Mayer, J. M. Oxygen Reduction by Homogeneous Molecular Catalysts and Electrocatalysts. *Chemical Reviews* **2018,** 118 (5), 2340-2391 DOI: 10.1021/acs.chemrev.7b00542.
4. Machan, C. W. Advances in the Molecular Catalysis of Dioxygen Reduction. *ACS Catalysis* **2020,** 10 (4), 2640-2655 DOI: 10.1021/acscatal.9b04477.
5. Solomon, E. I.; Goudarzi, S.; Sutherlin, K. D. O2 Activation by Non-Heme Iron Enzymes. *Biochemistry* **2016,** 55 (46), 6363-6374 DOI: 10.1021/acs.biochem.6b00635.
6. Solomon, E. I.; Stahl, S. S. Introduction: Oxygen Reduction and Activation in Catalysis. *Chemical Reviews* **2018,** 118 (5), 2299-2301 DOI: 10.1021/acs.chemrev.8b00046.
7. Huang, X.; Groves, J. T. Oxygen Activation and Radical Transformations in Heme Proteins and Metalloporphyrins. *Chemical Reviews* **2018,** 118 (5), 2491-2553 DOI: 10.1021/acs.chemrev.7b00373.
8. Hong, S.; Lee, Y.-M.; Ray, K.; Nam, W. Dioxygen activation chemistry by synthetic mononuclear nonheme iron, copper and chromium complexes. *Coordination Chemistry Reviews* **2017,** 334, 25-42 DOI: https://doi.org/10.1016/j.ccr.2016.07.006.
9. Bhunia, S.; Ghatak, A.; Dey, A. Second Sphere Effects on Oxygen Reduction and Peroxide Activation by Mononuclear Iron Porphyrins and Related Systems. *Chemical Reviews* **2022,** 122 (14), 12370-12426 DOI: 10.1021/acs.chemrev.1c01021.
10. Campos-Martin, J. M.; Blanco-Brieva, G.; Fierro, J. L. G. Hydrogen peroxide synthesis: An outlook beyond the anthraquinone process. *Angewandte Chemie - International Edition* **2006,** 45 (42), 6962-6984 DOI: 10.1002/anie.200503779.
11. Kiani, M.; Tian, X. Q.; Zhang, W. Non-precious metal electrocatalysts design for oxygen reduction reaction in polymer electrolyte membrane fuel cells: Recent advances, challenges and future perspectives. *Coordination Chemistry Reviews* **2021,** 441, 213954 DOI: https://doi.org/10.1016/j.ccr.2021.213954.
12. Pegis, M. L.; Martin, D. J.; Wise, C. F.; Brezny, A. C.; Johnson, S. I.; Johnson, L. E.; Kumar, N.; Raugei, S.; Mayer, J. M. Mechanism of Catalytic O2 Reduction by Iron Tetraphenylporphyrin. *Journal of the American Chemical Society* **2019,** 141 (20), 8315-8326 DOI: 10.1021/jacs.9b02640.
13. Zhang, R.; Warren, J. J. Recent Developments in Metalloporphyrin Electrocatalysts for Reduction of Small Molecules: Strategies for Managing Electron and Proton Transfer Reactions. *ChemSusChem* **2021,** 14 (1), 293-302 DOI: https://doi.org/10.1002/cssc.202001914.
14. Phung, Q. M.; Pierloot, K. The dioxygen adducts of iron and manganese porphyrins: electronic structure and binding energy. *Physical Chemistry Chemical Physics* **2018,** 20 (25), 17009-17019 DOI: 10.1039/C8CP03078B.
15. Zaragoza, J. P. T.; Goldberg, D. P. In *Dioxygen-dependent Heme Enzymes*; The Royal Society of Chemistry: 2019; pp 1-36.
16. VanAtta, R. B.; Strouse, C. E.; Hanson, L. K.; Valentine, J. S. Peroxo(tetraphenylporphinato)manganese(III) and chloro(tetraphenylporphinato)manganese(II) anions. Synthesis, crystal structures, and electronic structures. *Journal of the American Chemical Society* **1987,** 109 (5), 1425-1434 DOI: 10.1021/ja00239a024.
17. Passard, G.; Dogutan, D. K.; Qiu, M.; Costentin, C.; Nocera, D. G. Oxygen Reduction Reaction Promoted by Manganese Porphyrins. *ACS Catalysis* **2018,** 8 (9), 8671-8679 DOI: 10.1021/acscatal.8b01944.
18. Gennari, M.; Brazzolotto, D.; Pécaut, J.; Cherrier, M. V.; Pollock, C. J.; Debeer, S.; Retegan, M.; Pantazis, D. A.; Neese, F.; Rouzières, M.; Clérac, R.; Duboc, C. Dioxygen Activation and Catalytic Reduction to Hydrogen Peroxide by a Thiolate-Bridged Dimanganese(II) Complex with a Pendant

Thiol. *Journal of the American Chemical Society* **2015,** 137 (26), 8644-8653 DOI: 10.1021/jacs.5b04917.
19. Hamilton, G. A.; Revesz, A. Oxidation by Molecular Oxygen. IV. A Possible Model Reaction for Some Amine Oxidases1-3. *Journal of the American Chemical Society* **1966,** 88 (9), 2069-2070 DOI: 10.1021/ja00961a054.
20. Evans, D. F.; Sheriff, T. S. The production of hydrogen peroxide from dioxygen and hydroxylamine catalysed by manganese complexes. *J. Chem. Soc., Chem. Commun.* **1985,** (20), 1407-1408 DOI: 10.1039/C39850001407.
21. Shook, R. L.; Peterson, S. M.; Greaves, J.; Moore, C.; Rheingold, A. L.; Borovik, A. S. Catalytic Reduction of Dioxygen to Water with a Monomeric Manganese Complex at Room Temperature. *Journal of the American Chemical Society* **2011,** 133 (15), 5810-5817 DOI: 10.1021/ja106564a.
22. Hooe, S. L.; Rheingold, A. L.; Machan, C. W. Electrocatalytic Reduction of Dioxygen to Hydrogen Peroxide by a Molecular Manganese Complex with a Bipyridine-Containing Schiff Base Ligand. *Journal of the American Chemical Society* **2018,** 140 (9), 3232-3241 DOI: 10.1021/jacs.7b09027.
23. Hooe, S. L.; Machan, C. W. Dioxygen Reduction to Hydrogen Peroxide by a Molecular Mn Complex: Mechanistic Divergence between Homogeneous and Heterogeneous Reductants. *Journal of the American Chemical Society* **2019,** 141 (10), 4379-4387 DOI: 10.1021/jacs.8b13373.
24. Nichols, A. W.; Kuehner, J. S.; Huffman, B. L.; Miedaner, P. R.; Dickie, D. A.; Machan, C. W. Reduction of dioxygen to water by a Co(N2O2) complex with a 2,2'-bipyridine backbone. *Chemical Communications* **2021,** 57, 516-519 DOI: 10.1039/d0cc06763f.
25. Nichols, A. W.; Cook, E. N.; Gan, Y. J.; Miedaner, P. R.; Dressel, J. M.; Dickie, D. A.; Shafaat, H. S.; Machan, C. W. Pendent Relay Enhances H2O2 Selectivity during Dioxygen Reduction Mediated by Bipyridine-Based Co–N2O2 Complexes. *Journal of the American Chemical Society* **2021,** 143 (33), 13065-13073 DOI: 10.1021/jacs.1c03381.
26. Hooe, S. L.; Cook, E. N.; Reid, A. G.; Machan, C. W. Non-covalent assembly of proton donors and p- benzoquinone anions for co-electrocatalytic reduction of dioxygen. *Chemical Science* **2021,** 12 (28), 9733-9741 DOI: 10.1039/d1sc01271a.
27. Claude, P. Paramagnetic Susceptibility by NMR: The "Solvent Correction" Removed for Large Paramagnetic Molecules. *Journal of Chemical Education* **1997,** 74 (7), 815-816 DOI: https://doi.org/10.1021/ed074p815.
28. Bain, G. A.; Berry, J. F. Diamagnetic corrections and Pascal's constants. *Journal of Chemical Education* **2008,** 85 (4), 532-536 DOI: 10.1021/ed085p532.
29. Nichols, A. W.; Hooe, S. L.; Kuehner, J. S.; Dickie, D. A.; Machan, C. W. Electrocatalytic CO2 Reduction to Formate with Molecular Fe(III) Complexes Containing Pendent Proton Relays. *Inorganic Chemistry* **2020,** 59 (9), 5854-5864 DOI: 10.1021/acs.inorgchem.9b03341.
30. Saba, S.; Hernandez, R.; Choy, C. C.; Carta, K.; Bennett, Y.; Bondi, S.; Kolaj, S.; Bennett, C. A simple and efficient one-step protocol for the preparation of alkyl-substituted ammonium tetrafluoroborate and hexafluorophosphate salts. *Journal of Fluorine Chemistry* **2013,** 153, 168-171 DOI: https://doi.org/10.1016/j.jfluchem.2013.05.007.
31. Shivapurkar, R.; Jeannerat, D. Determination of the relative pKa's of mixtures of organic acids using NMR titration experiments based on aliased 1H–13C HSQC spectra. *Analytical Methods* **2011,** 3 (6), 1316-1322 DOI: 10.1039/C0AY00771D.
32. Zanello, P.; The Royal Society of Chemistry: Cambridge, UK, 2003; pp 49-135.
33. Anson, C. W.; Stahl, S. S. Cooperative Electrocatalytic O2 Reduction Involving Co(salophen) with p-Hydroquinone as an Electron–Proton Transfer Mediator. *J. Am. Chem. Soc.* **2017,** 139 (51), 18472-18475 DOI: 10.1021/jacs.7b11362.
34. Frisch, M. J.; Trucks, G. W.; Schlegel, H. B.; Scuseria, G. E.; Robb, M. A.; Cheeseman, J. R.; Scalmani, G.; Barone, V.; Petersson, G. A.; Nakatsuji, H.; Li, X.; Caricato, M.; Marenich, A. V.; Bloino, J.; Janesko, B. G.; Gomperts, R.; Mennucci, B.; Hratchian, H. P.; Ortiz, J. V.; Izmaylov, A. F.; Sonnenberg, J. L.; Williams-Young, D.; Ding, F.; Lipparini, F.; Egidi, F.; Goings, J.; Peng, B.; Petrone, A.; Henderson, T.; Ranasinghe, D.; Zakrzewski, V. G.; Gao, J.; Rega, N.; Zheng, G.; Liang,

W.; Hada, M.; Ehara, M.; Toyota, K.; Fukuda, R.; Hasegawa, J.; Ishida, M.; Nakajima, T.; Honda, Y.; Kitao, O.; Nakai, H.; Vreven, T.; Throssell, K.; J. A. Montgomery, J.; Peralta, J. E.; Ogliaro, F.; Bearpark, M. J.; Heyd, J. J.; Brothers, E. N.; Kudin, K. N.; Staroverov, V. N.; Keith, T. A.; Kobayashi, R.; Normand, J.; Raghavachari, K.; Rendell, A. P.; Burant, J. C.; Iyengar, S. S.; Tomasi, J.; Cossi, M.; Millam, J. M.; Klene, M.; Adamo, C.; Cammi, R.; Ochterski, J. W.; Martin, R. L.; Morokuma, K.; Farkas, O.; Foresman, J. B.; Fox, D. J. *Gaussian 16, Revision B.01*, Gaussian, Inc.: Wallingford CT, 2016.

35. Becke, A. D. Density-functional thermochemistry. III. The role of exact exchange. *The Journal of Chemical Physics* **1993,** 98 (7), 5648-5652 DOI: 10.1063/1.464913.
36. Lee, C.; Yang, W.; Parr, R. G. Development of the Colle-Salvetti correlation-energy formula into a functional of the electron density. *Physical Review B* **1988,** 37 (2), 785-789.
37. Vosko, S. H.; Wilk, L.; Nusair, M. Accurate spin-dependent electron liquid correlation energies for local spin density calculations: a critical analysis. *Canadian Journal of Physics* **1980,** 58 (8), 1200-1211 DOI: 10.1139/p80-159.
38. Stephen, P. J.; Devlin, F. J.; Chabalowski, C. F.; Frisch, M. J. Ab Initio Calculation of Vibrational Absorption and Circular Dichroism Spectra Using Density Functional Force Fields. *The Journal of Physical Chemistry* **1994,** 98 (45), 11623-11627.
39. Weigend, F.; Ahlrichs, R. Balanced basis sets of split valence, triple zeta valence and quadruple zeta valence quality for H to Rn: Design and assessment of accuracy. *Physical Chemistry Chemical Physics* **2005,** 7 (18), 3297-3305 DOI: 10.1039/b508541a.
40. Weigend, F. Accurate Coulomb-fitting basis sets for H to Rn. *Physical Chemistry Chemical Physics* **2006,** 8 (9), 1057-1065 DOI: 10.1039/b515623h.
41. Grimme, S.; Antony, J.; Ehrlich, S.; Krieg, H. A consistent and accurate ab initio parametrization of density functional dispersion correction (DFT-D) for the 94 elements H-Pu. *Journal of Chemical Physics* **2010,** 132 (15), 154104-154104 DOI: 10.1063/1.3382344.
42. Grimme, S.; Ehrlich, S.; Goerigk, L. Effect of the damping function in dispersion corrected density functional theory. *Journal of Computational Chemistry* **2011,** 32 (7), 1456-1465 DOI: https://doi.org/10.1002/jcc.21759.
43. Neese, F. Software update: The ORCA program system—Version 5.0. *WIREs Computational Molecular Science* **2022,** 12 (5), e1606 DOI: https://doi.org/10.1002/wcms.1606.
44. Mardirossian, N.; Head-Gordon, M. ωB97M-V: A combinatorially optimized, range-separated hybrid, meta-GGA density functional with VV10 nonlocal correlation. *The Journal of Chemical Physics* **2016,** 144 (21), 214110 DOI: 10.1063/1.4952647.
45. Hellweg, A.; Hättig, C.; Höfener, S.; Klopper, W. Optimized accurate auxiliary basis sets for RI-MP2 and RI-CC2 calculations for the atoms Rb to Rn. *Theoretical Chemistry Accounts* **2007,** 117 (4), 587-597 DOI: 10.1007/s00214-007-0250-5.
46. Caldeweyher, E.; Bannwarth, C.; Grimme, S. Extension of the D3 dispersion coefficient model. *The Journal of Chemical Physics* **2017,** 147 (3), 034112 DOI: 10.1063/1.4993215.
47. Caldeweyher, E.; Ehlert, S.; Hansen, A.; Neugebauer, H.; Spicher, S.; Bannwarth, C.; Grimme, S. A generally applicable atomic-charge dependent London dispersion correction. *The Journal of Chemical Physics* **2019,** 150 (15), 154122 DOI: 10.1063/1.5090222.
48. Najibi, A.; Goerigk, L. DFT-D4 counterparts of leading meta-generalized-gradient approximation and hybrid density functionals for energetics and geometries. *Journal of Computational Chemistry* **2020,** 41 (30), 2562-2572 DOI: https://doi.org/10.1002/jcc.26411.
49. Chaau Yan Poon, P.; Dedushko, M. A.; Sun, X.; Yang, G.; Toledo, S.; Hayes, E. C.; Johansen, A.; Piquette, M. C.; Rees, J. A.; Stoll, S.; Rybak-akimova, E.; Kovacs, J. A. How Metal Ion Lewis Acidity and Steric Properties Influence the Barrier to Dioxygen Binding, Peroxo O-O Bond Cleavage, and Reactivity. *Journal of the American Chemical Society* **2019,** 141, 15046-15057 DOI: 10.1021/jacs.9b04729.

50. Li, J.-Z.; Hu, W.; Wang, Y.; Zhong, J.-B.; Li, S.-X. A Kinetic Study of Phenol Oxidation with H2O2 Catalysed by Crowned Schiff Base Mn(Iii) Complexes in Micellar Media. *Progress in Reaction Kinetics and Mechanism* **2012,** 37 (1), 30-41 DOI: 10.3184/146867812X13242290723318.
51. Broughton, D. B.; Wentworth, R. L. Mechanism of Decomposition of Hydrogen Peroxide Solutions with Manganese Dioxide. I. *Journal of the American Chemical Society* **1947,** 69 (4), 741-744 DOI: 10.1021/ja01196a003.